Membrane-related Specializations Associated with Acetylcholine Receptor Aggregates Induced by Electric Fields

PAUL W. LUTHER and H. BENJAMIN PENG
Department of Anatomy, University of Illinois at Chicago, Chicago, Illinois 60680

ABSTRACT The localization of membrane-associated specializations (basal lamina and cytoplasmic density) at sites of acetylcholine receptor (AChR) aggregation is consistent with an involvement of these structures in receptor stabilization. We investigated the occurrence of these specializations in association with AChR aggregates that develop at the cathode-facing edge of *Xenopus* muscle cells during exposure to a DC electric field. The cultures were labeled with a fluorescent conjugate of α-bungarotoxin and the receptor distribution on selected cells was determined before and after exposure to the field. In thin sections taken from the same cells, the cathode-facing edge was characterized by plaques of basal lamina and cytoplasmic density co-extensive with sarcolemma of increased density. In sections cut in a plane similar to the fluorescence image, it was possible to demonstrate that the specializations were concentrated at areas of field-induced AChR aggregation, and at receptor clusters existing on control cells. This finding further indicates that these structures participate in AChR stabilization, and that the mechanisms involved in AChR aggregation that result from field exposure and nerve contact may be similar.

During the development of the neuromuscular junction, stable aggregates of acetylcholine receptors (AChR)[1] form within the pre-existing diffuse receptor population on the muscle cell (1, 2) and may result from the redistribution of surface AChR (3). In addition, the postsynaptic sarcolemma develops structural specializations, which include regions of increased membrane density co-extensive with a well-developed basal lamina and cytoplasmic dense layer (4–6). This association is maintained at the mature junction, where the specializations and AChR aggregates are co-localized at the crests of the postsynaptic folds (7, 8). A similar co-localization of AChR and these specializations has been demonstrated at AChR clusters that form on non-innervated muscle cells in culture (9), and at those induced by nerve extracts (10) and polycation-coated beads (11). In these cases, aggregation also involves the redistribution of pre-existing AChR into stable aggregates (10–12). Because dispersed AChR undergo lateral diffusion in the membrane (13, 14), the stability of these aggregates indicates that a mechanism to restrict receptor motion exists. Considering the consistent localization of the described specializations at sites of AChR aggregation, it is possible that they may be related to this mechanism.

The exposure of cultured muscle cells to DC electric fields also causes the redistribution of surface AChR into aggregates (15). It has been proposed that the field-induced translocation of the receptors is the result of electrophoresis (15) or electroosmotic flow (16) resulting from the voltage gradient imposed along the cell surface. However, the resulting aggregates are stable against lateral diffusion following termination of the field (15). It was therefore of interest to determine if postsynaptic-like specializations are also associated with these aggregates. In this study, fluorescence microscopy was used to monitor the distribution of AChR on cultured *Xenopus* muscle cells before and after exposure to a 7.5 V/cm electric field; the same cells were then thin-sectioned and examined by electron microscopy. The results demonstrate that the specializations were present and localized at areas where AChR aggregates had formed during exposure to the field. A preliminary account of these findings has appeared (17).

[1] *Abbreviations used in this paper*: AChR, acetylcholine receptor; TMR-αBTX, tetramethylrhodamine-conjugated α-bungarotoxin.

MATERIALS AND METHODS

Cell Culture: Cultures of myotomal muscle cells were prepared from stage 20–22 *Xenopus laevis* embryos (18) as has been described (19, 20) and plated on uncoated glass coverslips in a medium consisting of 10% L-15 (Leibovitz) and 1% fetal bovine serum (Gibco Laboratories, Grand Island, NY) in Steinberg's saline (60 mM NaCl, 0.67 mM KCl, 0.83 mM $MgSO_4$, 0.34 mM $Ca(NO_3)_2$, 10 mM HEPES, pH 7.4). The cells were maintained at 20°C and exposed to the electric field after 2–4 d of culture.

Fluorescence Microscopy: Cultures were labeled with α-bungarotoxin conjugated with tetramethylrhodamine (TMR-αBTX) (21) for 30–60 min and washed in several changes of culture medium. Fluorescence was observed with a Leitz Orthoplan microscope using a 100-W mercury arc lamp and epifluorescence illumination through a 63×, NA 1.4, objective and N2.1 filter cube. The prefield receptor distribution on selected cells was observed and recorded using a Cohu 4410 silicon intensified target (SIT) video camera (Cohu Inc., Electronics Div., San Diego, CA), which permitted reduction of the excitation illumination with a 6.3% transmittance neutral density filter in order to minimize bleaching of the fluorophore as well as possible adverse effects on the cells related to its excitation (22). Selected cells were bipolar, oriented within 45° of perpendicular to the applied field, and without interactions with other cells. The postfield receptor distribution on the same cells was photographed with an Olympus OM-2 camera using Kodak Tri-X film without reduction of the excitation illumination, to maximize resolution.

Field Application: Procedures were adapted from those used previously (15, 23). We constructed open rectangular chambers by attaching coverglass strips to microscope slides with silicone cement. The culture coverglass was inverted over the opening and sealed to the chamber with dental wax, thereby enclosing an area of 0.2 × 10 × 54 mm^3 with a small open extension at each end. Cylindrical glass reservoirs were sealed around the openings with silicon grease, and current was applied to these through 15-cm 2% agar-Steinberg's saline bridges, which isolated the chamber from beakers containing Ag-AgCl electrodes immersed in Steinberg's saline and connected to a power supply. This arrangement minimized manipulations by permitting pre- and postfield microscopic observations while the cultures were on the chambers. Application of 1.1-mA of current, as measured by an ammeter in series with the power supply, resulted in a calculated field strength of 7.5 V/cm in the chamber, which corresponds to a 20-mV potential gradient across a typical, 25-μm-wide cell. Field durations of 3–4 h were used in these experiments. Controls were treated similarly, but subjected to a 3–4-h incubation period (without field exposure).

Electron Microscopy: After postfield photography, the cultures were removed from the chambers under Steinberg's saline and fixed in 2% glutaraldehyde with 10 mM $Ca(NO_3)_2$ in 50 mM cacodylate buffer (pH 7.2) for 2 h, postfixed with 1% OsO_4 in the same buffer, en bloc stained with 1% uranyl acetate in 50 mM acetate buffer (pH 5.5), dehydrated through an ethanol series, and embedded in Epon 812. After curing, the Epon was softened by immersion in a 70°C water bath, separated from the coverglass with a scalpel blade, and dried in a vacuum dessicator. For sectioning parallel to the substrate, the selected cells were relocated, cut out, and glued to Epon blanks with Epoxy 907 (Miller-Stephenson Co., Chicago, IL). For cross sections, the blocks were secured directly into the microtome chuck; after trimming, the cell could be sufficiently resolved by light microscopy to identify the level of sectioning. Thin sections were collected on Formvar-coated single-slot grids, stained with uranyl acetate and lead citrate, and observed with a JEOL 100s electron microscope operating at 60 kV. The results are based on 17 cells that were prefield mapped, subjected to the field (or control incubation), postfield mapped, and thin-sectioned through identified areas of AChR aggregation.

RESULTS

Field-induced Redistribution of AChR

It has been demonstrated that exposure of cultured *Xenopus* myocytes to DC electric fields causes the redistribution of AChR into aggregates at the cathode-facing edge of the cells (15, 24). In the following experiments, this redistribution was observed directly by labeling the culture with TMR-αBTX and recording the prefield AChR distribution on selected cells using video-intensified fluorescence microscopy (Fig. 1 *B*). Following exposure to a 3-h 7.5 V/cm field, the same cells were relocated and examined by conventional fluorescence microscopy, which revealed new fluorescent areas at the cathode-facing edge of the myocytes (Fig. 1 *C*). In contrast to the single cathodal aggregate forming on the spherical "myoballs" used in previous investigations (24), the bipolar cells used in these experiments were characterized by multiple cathodal aggregates, which occurred as discrete patches separated by nonfluorescing extents of the cathode-facing edge (Fig. 1 *C*). A speckled substructure in the micrometer-to-submicrometer range was evident within these patches. These characteristics were particularly evident through the variation in fluorescence pattern that resulted upon altering the plane of focus, thereby demonstrating discontinuity of the aggregates in the vertical plane. Receptor aggregates were not observed to form at noncathodal locations during field exposure, or at any location on cells subjected to 3-h control incubations (Fig. 2, *B* and *C*). Alterations in the position or substructure of pre-existing AChR aggregates on field-exposed or control cells were not observed.

Specializations Associated with the Cathode-facing Edge

To determine if field exposure had resulted in ultrastructural modification of the cathode-facing edge in association with AChR redistribution, selected cells were thin-sectioned parallel to the substrate and examined by electron microscopy. For this evaluation, it was necessary to minimize interference from specializations associated with pre-existing (i.e., not field-induced) AChR aggregates. Therefore, only cells that had no observable fluorescence at the presumptive cathode- and anode-facing edges prior to field exposure were sectioned. At magnifications as low as 5,000 the occurrence of discrete dense areas at the cathode-facing edge was evident (Fig. 3). Like the cathodal fluorescence described above, these were distributed discontinuously along the sarcolemma, comprising extents in the micron-to-submicron range (0.7 ± 0.6 μm,

FIGURE 1 AChR aggregates and membrane specializations in a field-exposed muscle cell, cathode towards the left. (*A*) Phase-contrast micrograph of cell after field exposure. *V*, vacuole; *L*, lipid inclusion; *Y*, yolk granule. (*B*) Video-intensified fluorescence micrograph prior to field application. Note the absence of AChR aggregates along the future cathodal edge. (*C*) Postfield fluorescence micrograph of the same cell. Note the numerous AChR aggregates that have developed at the cathode-facing edge of the cell, three of which are indicated (arrows). Structures visible by autofluorescence are also indicated. (*D*) Thin section taken at a level similar to the plane of focus of *C*, as evidenced by the indicated structures. Small arrows indicate the location of the following enlargements. (*E*) Cathode-facing sarcolemma in the vicinity of aggregate No. 1. Note the presence of dense areas (arrows). (*F*) Enlargement of the upper specialization in *E*, which demonstrates that the specializations consist of co-extensive basal lamina (*BL*), dense membrane (*DM*), and submembranous density (*SMD*). (*G*) Specialized sarcolemma in the vicinity of aggregate No. 2; one patch is partially enclosed by an extension from the cell surface (arrow). (*H*) Specialized sarcolemma in the vicinity of aggregate No. 3. Basal lamina is co-extensive with the lower specializations but not evident at the upper one. *MT*, microtubule. (*I*) Cathode-facing sarcolemma from an area where AChR aggregation is less extensive. Only two small areas of specialization are evident (arrows). (*A–D*) × 750. (*E*) × 22,000. (*F*) × 80,000. (*G*) × 36,000. (*H*) × 50,000. (*I*) × 21,000.

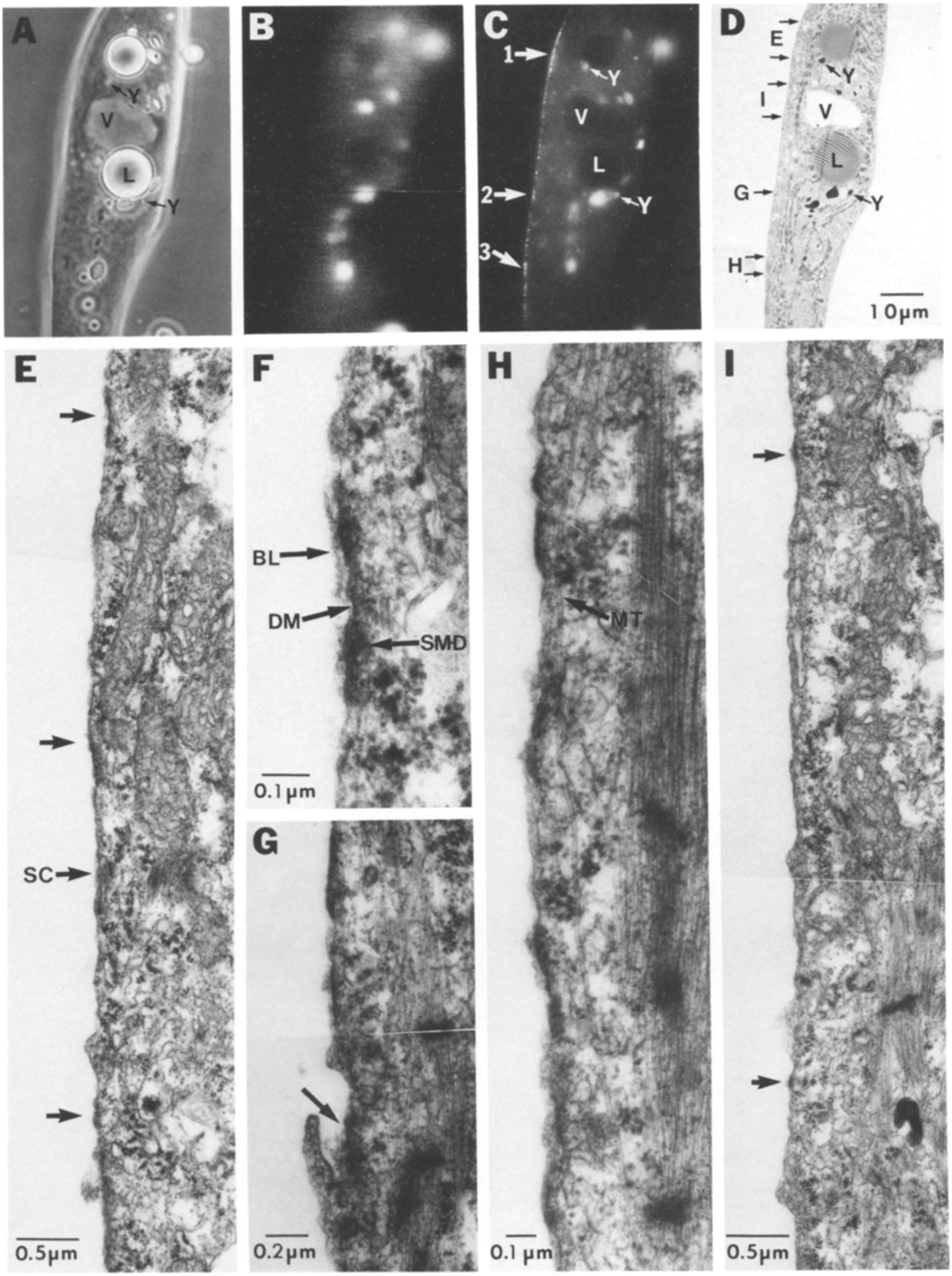
A
Y
V
L
Y
B
C
1
Y
V
L
2
Y
3
D
E
Y
I
V
L
G
Y
H
10μm
E
SC
0.5μm
F
BL
DM
SMD
0.1μm
G
0.2μm
H
MT
0.1μm
I
0.5μm

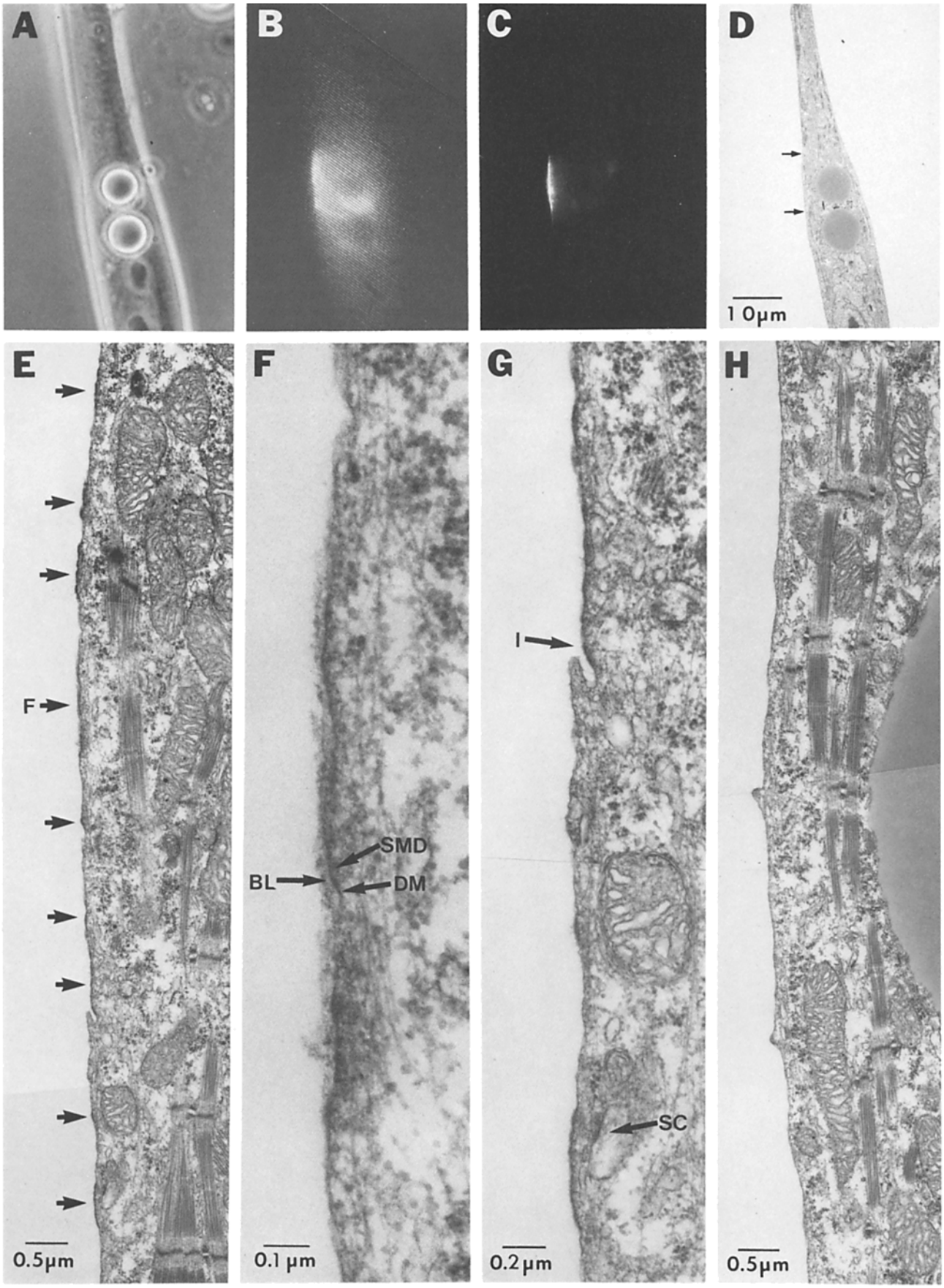

FIGURE 2 Specializations associated with control AChR aggregates. (*A*) Phase-contrast micrograph of cell after control incubation. (*B*) Video-intensified fluorescence microscopy prior to incubation. A large AChR aggregate is located on the edge of the cell. (C) Postincubation fluorescence micrograph of the same cell. No alterations in the position of the aggregate are apparent. (*D*) Thin section from the same cell. Arrows indicate the region enlarged in *E*. (*E*) Several areas of increased density are evident at the edge of the cell in the area of AChR aggregation (arrows). (*F*) High magnification of the density indicated in *E* reveals basal lamina (*BL*), dense membrane (*DM*), and submembranous density (*SMD*). (*G*) High magnification of the lower dense areas in *E*. Specializations associated with a surface invagination (*I*) and subsurface cisterna (*SC*) are indicated. (*H*) Sarcolemma from an area without AChR aggregation; no specializations are apparent. (*A–D*) × 850. (*E*) 15,000. (*F*) × 80,000. (G) × 36,000. (*H*) × 14,000.

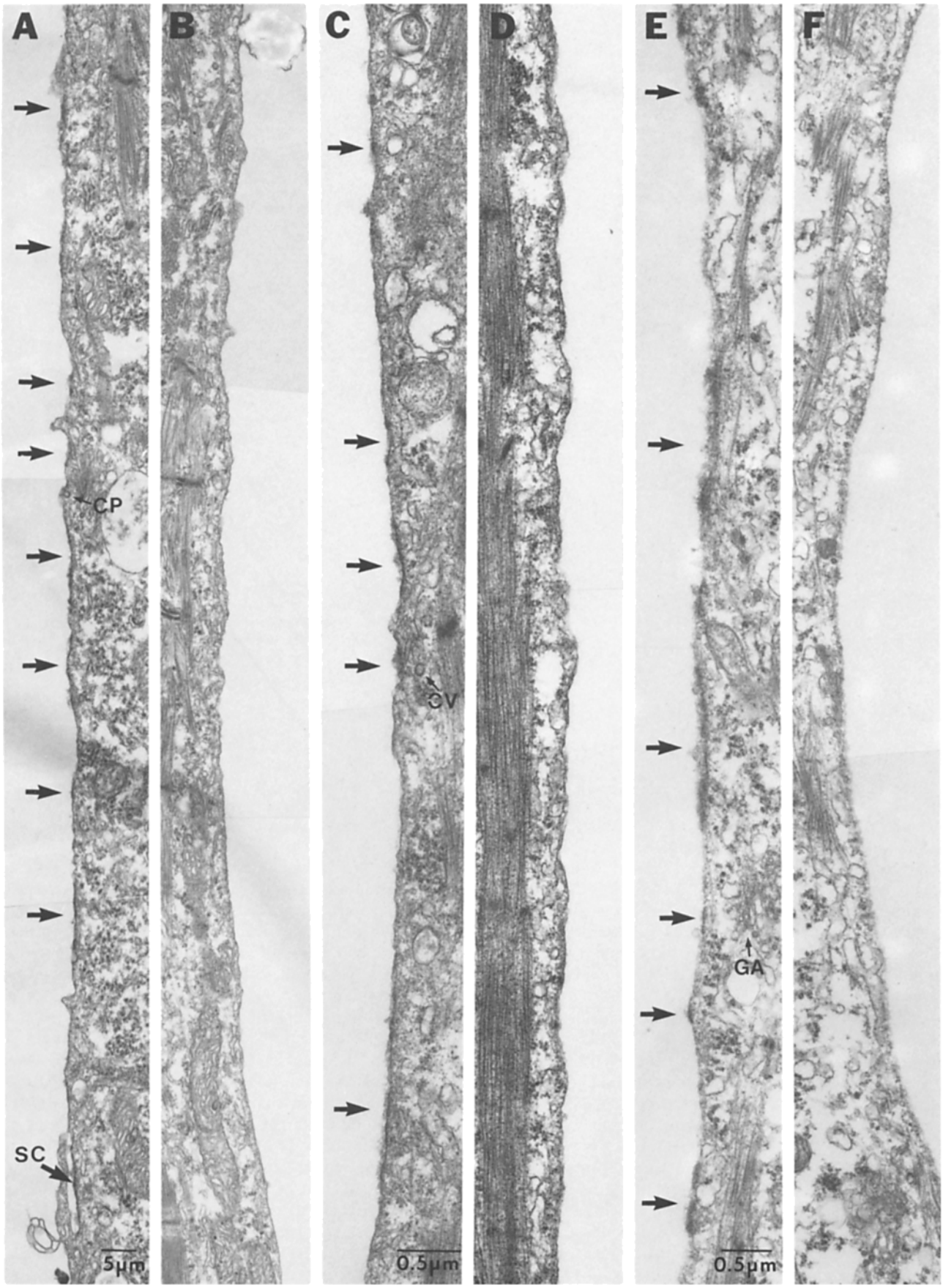

FIGURE 3 Comparison of cathode- and anode-facing edges of field-exposed cells. In all examples, prefield video-intensified fluorescence microscopy revealed no AChR aggregates at the presumptive cathode-facing edge, whereas numerous cathodal AChR aggregates were present following field exposure. Note that a large number of dense areas (arrows) are present at the cathode-facing edges (*A*, *C*, and *E*), but none are evident at the anode-facing edges of the same cells (*B*, *D*, and *F*), shown at the same magnification. *CP*, coated pit; *CV*, coated vesicle; *GA*, Golgi apparatus. *SC* indicates a dense area located on a subsurface cistern. (*A* and *B*) × 1,200. (C and *D*) × 22,000. (*E* and *F*) × 17,000.

TABLE I

Correlations between TMR-αBTX Fluorescence and Fine Structures

Cell	Fluorescence*		Density‡			Density§			Structures‖					
	C	A	C	A	C/A	F	NF	F/NF	Area	BL	SMD	MT	CV	GA
	a	b	c	d	e	f	g	h	i	j	k	l	m	n
Field-exposed cells														
1	1.7	0	0.5	0.1	5.0	1.2	0.4	3.0	D	8.3	8.7	0.0	0.0	0.0
									ND	0.7	1.4	0.9	0.4	0.0
2	2.3	0	0.9	0.4	2.3	3.3	0.2	16.5	D	6.5	7.5	2.1	0.7	0.7
									ND	0.4	0.2	2.2	0.0	0.0
3	1.9	0	0.9	0.0	—	3.4	0.5	6.8	D	3.6	6.5	0.0	0.0	0.6
									ND	0.3	0.3	0.0	0.0	0.0
4	2.4	0	1.2	0.2	6.0	4.1	0.6	6.8	D	6.9	8.4	9.9	3.0	1.0
									ND	0.4	0.3	0.8	0.4	0.0
5	2.9	0	2.4	0.2	12.0	—	—	—	D	4.3	8.4	6.3	0.7	0.0
									ND	1.3	0.7	0.5	0.0	0.0
Pooled¶	2.3	0	1.0	0.2	5.0	3.0	0.4	7.5	D	5.8	8.0	3.4	0.8	0.5
									ND	0.6	0.5	1.0	0.2	0.0
									D/ND	9.7	16.0	3.4	4.0	—
Control cells														
6						3.9	0.0	—	D	3.9	9.8	2.9	0.0	0.0
									ND	0.1	0.2	0.3	0.0	0.0
7						4.6	0.2	23.0	D	5.8	8.8	0.0	0.0	0.0
									ND	0.5	0.3	0.3	0.0	0.0
Pooled¶						4.2	0.1	42.0	D	4.8	9.4	1.7	0.0	0.0
									ND	0.3	0.3	0.8	0.0	0.0
									D/ND	16.0	31.3	2.1	—	—

* *C*, cathode-facing edge; *A*, anode-facing edge. Based on the measurement of all fluorescent areas at the cell edges and the total extent of the edge within the area of fluorescence illumination taken from 1,100× micrographs. Data are expressed as length per 10 μm of sarcolemma in columns *a–d* and *f–g*.

‡ Based on the measurement of distinct dense areas exceeding 0.25 μm, and the total length of the evaluated edge on 5,000–10,000× micrographs. The ends of the cells, where the section was tangential to the sarcolemma, were not evaluated.

§ *F*, fluorescing; *NF*, nonfluorescing areas of sarcolemma. Based on the same measurements as in columns c and *d*, but categorized as within or outside highly fluorescent areas. The latter were delimited on the electron micrograph by superimposing the fluorescence image based on landmarks visible in both.

‖ *BL*, basal lamina; *SMD*, submembranous density; *MT*, microtubules; *CV*, coated vesicles and pits; *GA*, Golgi apparatus; *D*, dense membrane; *ND*, nondense membrane. Based on measurements made within and outside the dense areas identified for columns c and *d*, but on 25,000–30,000× micrographs. To insure distinction of these areas, sarcolemma within 1 μm of dense areas was not evaluated. The total extents of basal lamina and submembranous density within an area were measured and expressed as occurrence per 10 μm of sarcolemma. Microtubules, coated vesicles, and Golgi apparatus were scored if within 75, 250, and 500 nm of the sarcolemma, respectively, and expressed as observations per 10 μm of sarcolemma.

¶ Indicates results calculated from the summed data obtained from individual cells.

mean ± SD, $n = 82$). These sometimes occurred in groups, and 24% exceeded 1 μm in length. Few dense areas were observed at the anode-facing sarcolemma; these were of a slightly smaller dimension (0.5 ± 0.3 μm, $n = 20$), and only one (5%) exceeded 1 μm in extent. The effect was quantitated by determining the total extent of density occurring along a cell edge (omitting the ends, where the section was tangential to the membrane), and expressing this as extent per 10 μm of the evaluated edge.

Individual and pooled results from the cathode- and anode-facing edges of five cells evaluated from ×5,000–10,000 micrographs are listed in Table I. In all of these cells, the extent of dense area occurring at the cathode-facing edge was elevated relative to that at the edge facing the anode (columns *c–e*, Table I) and at nonfluorescing edges of control cells (column *g*, cells 6 and 7). The actual fraction of the cathodal sarcolemma that was dense, and the ratio of this fraction to that of the respective anodal edge (column *e*), varied considerably between cells. When the measurements from all five cells were pooled, dense membrane was found to comprise ~10% of the cathode-facing sarcolemma, whereas <2% of the anode-facing membrane and of nonfluorescing edges of control cells appeared to be dense.

The similar distribution of density and AChR aggregates in field-exposed cells suggest a relationship between the phenomena; this is further implied by the observation that the occurrence of density along the cathode-facing edge was proportional to the occurrence of TMR-αBTX fluorescence along that edge (compare columns *a* and *c*, Table I). The spatial relationship between the distributions of densities and AChR aggregates was determined more precisely by delimiting the extent of highly fluorescent regions of the cell edge on electron micrographs and quantifying the occurrence of dense regions within and outside these areas. To perform this correlation it was necessary that the section (*a*) be taken from a plane similar to that of the fluorescence micrograph; (*b*) contain intracellular and extracellular landmarks that were also identifiable in the fluorescence image (Fig. 1, *C* and *D*), to permit determination of the plane of section and superimposition of the fluorescence and thin section images; and (*c*) be precisely parallel to the substrate. These criteria were met for the first four cells in Table I, and cell number 4 is shown in Fig. 1. The results indicate that the spatial distribution of AChR aggregates and densities are correlated, with the occurrence of densities being elevated eightfold in fluorescing areas relative to nonfluorescing regions (compare columns *f* and *g*, Table I). This is evident by comparing Fig. 1, *E–H*, which are electron micrographs of the fluorescent areas indicated in Fig. 1 *C*, with Fig. 1 *I*, which is of a low-fluorescence area. For comparison, two control cells that had AChR aggregates on a free edge of the cell (i.e., not substrate associated) were sectioned parallel to the substrate. In these, the elevated occur-

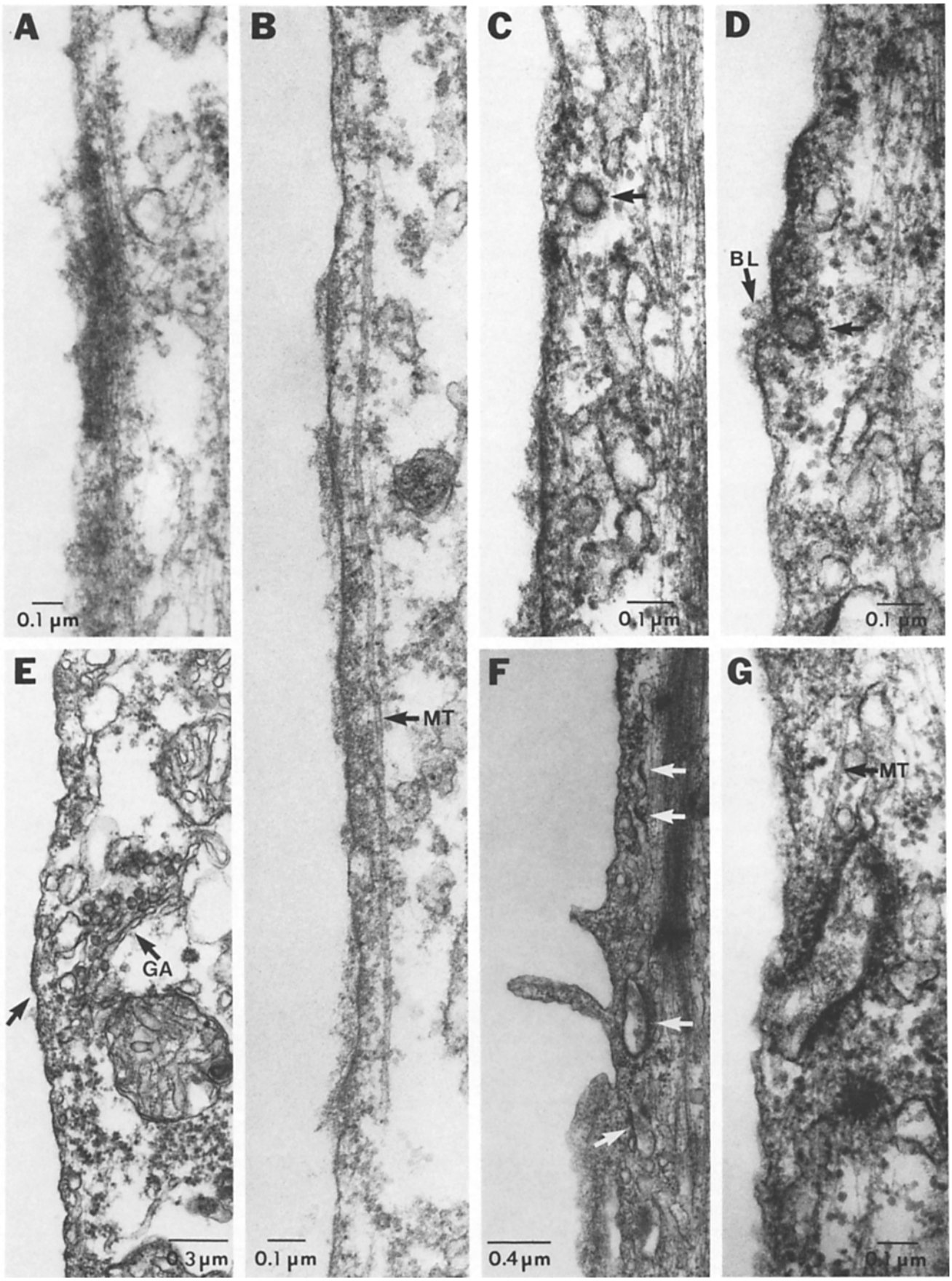

FIGURE 4 Specializations associated with field-induced AChR aggregates. (*A*) Tangential section of specialized area reveals microfilaments associated with the submembranous density. (*B*) A microtubule (*MT*) parallels a specialized region for several micrometers. (*C*) A coated vesicle (arrow) in the vicinity of a specialized region. (*D*) A coated pit (arrow) associated with the edge of a specialization. The contents of the pit appear continuous with basal lamina (*BL*). (*E*) A Golgi apparatus (*GA*) near a specialization (arrow). (*F*) Specializations on subsurface cisternae (arrows). (*G*) Specialization on a membrane invagination. (*A*) × 54,000. (*B*) 65,000. (*C*) × 80,000. (*D*) × 80,000. (*E*) × 33,000. (*F*) × 27,000. (*G*) × 70,000.

rence of dense patches in fluorescent regions of the edge was greater than that observed in field-exposed cells (Fig. 2*E* and column *f* for cells 6 and 7 in Table I). The intensity of TMR-αBTX fluorescence was also greater than in cathodal fluorescent areas, which further suggests a relationship between the dense areas and AChR aggregates.

High-magnification (25,000–30,000) micrographs of the cathodal dense areas identified in the above quantification were evaluated to determine their structural constitution. Quantification of the findings are listed in columns *i–n* of Table I. All of the densities were observed to result from the presence of a submembranous dense layer, generally in association with basal lamina and increased sarcolemmal density (Fig. 1*F*). This association varied from a precisely co-extensive and continuous patch of all three specializations to an intermittent disposition of the elements within the dense area in which their registration was less precise. Although in some cases the submembranous dense layer and dense sarcolemma occurred in the absence of basal lamina, basal lamina was rarely observed in the absence of the other specializations. The extent of these specializations within delimited dense areas is indicated in columns *j* and *k* of Table I. The submembranous density was substructured and irregular in thickness (40 ± 10 nm, $n = 62$) and appeared to impinge directly on the sarcolemma. The cytoplasmic surface of the structure merged indistinctly with cortical granular and filamentous structures. Basal lamina was observed at 91% of the identified dense areas and was also substructured and variable in thickness (45 ± 16 nm, $n = 55$). The substance generally appeared to impinge directly on the membrane, and a lamina lucida was rarely observed. The occurrence of dense membrane was difficult to assess as the sarcolemma was frequently obscured by the submembranous layer. However, at many locations the membrane density exceeded that of the submembranous structure, and its distinction from unspecialized sarcolemma was evident at most (55%) of the dense areas (Fig. 1*F*). Similar specializations were observed at dense areas in control cells (cells 6 and 7 in Table I and Fig. 2*F*), but they occurred infrequently in areas categorized as nondense in low-magnification observations of both field-exposed and control cells (Table I and Figs. 1*I* and 2*H*).

Several other specializations were sometimes observed to associate with dense areas. Specific examples of these are shown in Fig. 4, and others are indicated in Figs. 1–3. The frequency at which these structures were observed per 10 μm of dense membrane is indicated in columns *l–n* of Table I. Microtubules (diameter [*d*] = 21.4 ± 2.0 nm, $n = 15$) were observed within 75 nm of 34% of the dense areas, and in some cases paralleled these for several micrometers (Fig. 4*B*). Coated vesicles ($d = 81.5 \pm 3.0$ nm, $n = 4$) and coated pits were observed in association with 8% of the densities (Fig. 4, *C* and *D*). An array of lamellae and vesicles resembling Golgi apparatus was observed near 5% of the dense areas (Fig. 4*E*). The specificity of these associations is indicated by the frequency at which the structures were observed in relation to nondense sarcolemma (columns *l–n*, Table I). In addition, a direct association of the submembranous density with microfilaments ($d = 5.8 \pm 1.0$ nm, $n = 43$) was observed in 76% of dense areas evaluated at 80,000–90,000× (Fig. 4*A*). Finally, 9% of the dense areas were located in sarcolemmal invaginations (Fig. 4*G*) or subsurface cisternae (Fig. 4*F*); it is possible that the latter are actually cross-sectioned invaginations. In the control cells sectioned in this investigation, microtubules were observed in relation to 17% of the densities, and 17% of the dense areas were located in sarcolemmal invaginations or cisternae; however, associations with Golgi apparatus or coated vesicles were not observed.

In addition to the cells listed in Table I, seven field-exposed and three control cells were sectioned parallel to the substrate or cross-sectioned through identified field-induced or control AChR aggregates and evaluated qualitatively. The observations were consistent with those described above, except that (*a*) dense areas on the cathode-facing edge of field-exposed cells appeared less extensive in cross-sectioned cells, further indicating subunit structuring of the specializations, and (*b*) substrate-associated control aggregates were always associated with specializations on large cisternae or intensive membrane invaginations, which sometimes exceeded 0.5 μm.

DISCUSSION

This investigation indicates that the application of an electric field to cultured *Xenopus* myocytes results in the elaboration of membrane-associated structural specializations in addition to AChR aggregates at the cathode-facing edge of the cells, and that a temporal and spatial relationship exists between these phenomena. That both receptor aggregates and the specializations are elaborated within the 3–4-h duration of the field suggests a temporal association; this time scale is similar to that of their formation at developing neuromuscular contacts in vivo (4, 25). A spatial association is indicated by an increased concentration of the specialized dense areas within areas of AChR aggregation observed in correlated fluorescence and thin-section images. The structural characteristics of these specializations and the observed temporal and spatial relationships are similar to those observed at developing neuromuscular junctions and AChR aggregates in other systems (9–11), which may indicate a common mechanism for their elaboration as well as a functional relationship between AChR aggregation and the specializations.

A considerable amount of evidence can be extracted from the literature to support the contention that basal lamina or the submembranous density is involved in the stabilization of aggregated AChR. Rotary replication (26) and high-voltage or whole-mount electron microscopy (27, 28) have resolved the submembranous density into a filamentous network, and the impingement of these filaments upon the sarcolemma has been described (12, 29–31). Furthermore, immunological studies indicate that the subsynaptic sarcoplasm is distinguished by a number of cytoskeletal proteins, including the cytoplasmic isoforms of actin, vinculin, α-actinin, filamin, and an intermediate filament-like protein (32–34). The possibility of cytoskeletal-AChR interaction is also indicated by (*a*) the disposition of postsynaptic AChR correlates into rows as visualized by freeze-fracture and deep-etch replication (30, 31, 35), an arrangement which is consistent with attachment to underlying filaments; (*b*) the increased diffusional mobility of AChR in membrane blebs (36), which are presumably devoid of cytoskeletal interaction; (*c*) the capacity of Triton-X to extract aggregated AChR (37), which indicates that interactions between the receptor and extramembranous elements must exist; and (*d*) the ability of cytoskeletal disrupting agents to affect AChR aggregation and dispersal (38, 39), suggesting a functional relationship. Some of the above evidence is also consistent with an involvement of the associated basal lamina in the stabilization of aggregated AChR. This

substance also has a specialized molecular composition (40–42) and directly impinges on the sarcolemma (26, 29). Furthermore, isolated synaptic basal lamina is capable of inducing AChR aggregation (43–44). However, the involvement of either structure in AChR stabilization remains to be established. For example, associated basal lamina and submembranous densities are also co-localized at certain regions in the absence of AChR aggregation: at focal contacts (45), along the nonjunctional sarcolemma of slow muscle (46), and at the myotendinous junction (46, 47). Considering the tenacity of the neuromuscular contact (48), it is possible that the specializations are more relevant to the stabilization of the junction than of AChR. In this regard, it is interesting that the experimental induction of AChR aggregation with basal lamina (43), polycation-coated beads (11), silk thread and degenerating nerve (49), or substrate (12) requires cell surface contact with an exogenous substance. The induction of aggregation by nerve extracts and conditioned medium may be analogous if the active factor is a cell surface component, which is consistent with the ability of laminin and collagen V to stimulate its activity (50). The aggregation of AChR and development of associated specializations through exposure to the electric field may therefore be significant in that events are induced in the absence of such contact, which strengthens the argument for a functional association between the specializations and AChR stabilization.

The observed spatial coincidence between AChR aggregates and dense areas was not absolute. This may be the result of (*a*) an imperfect alignment of the thin-section and fluorescence images; (*b*) a disparity between the location or thickness of the plane of section and fluorescence plane of focus; or (*c*) the presence of unlabeled AChR aggregates (i.e., resulting from AChR externalized after prefield TMR-αBTX labeling), or aggregates smaller than the limit of resolution for fluorescence microscopy. Alternatively, a minority of AChR aggregates or dense areas may exist in the absence of the described association. Furthermore, this study does not establish whether the formation of specializations is precedent, coincident, or subsequent to that of the aggregate (i.e., within the 3-h field duration). Other investigators have observed specialized sarcolemma at which AChR labeling is partial or absent co-existing with labeled specializations (9, 10), which may indicate that the specializations precede aggregation, perhaps acting as a receptor "trap" (51). Considering the measured rate of AChR diffusion (13, 14), and possible electrophoretic effects (15), the time scale of electric field-induced aggregation does not conflict with this possibility.

The association of microtubules, coated vesicles, and cisternae with AChR aggregates has been observed in several systems. Microtubules have been observed in association with postsynaptic densities and the associated microfilaments (9, 11, 26), and colchicine inhibits receptor aggregation (12, 38, 52). (However, colchicine does not appear to affect field-induced AChR aggregation [15].) Coated vesicles are often associated with the specialized surface, and can be labeled with α-bungarotoxin conjugates (9, 53–54); these may represent a vector for the insertion or reuptake of AChR. Cisternae with basal lamina and submembranous density specializations have been observed in association with polycation-coated bead contacts (11) and acetylcholine esterase sites (55) in cultured *Xenopus* muscle cells. In terms of the current investigation, it is possible that intracellular structures such as these participate in the elaboration of the observed specializations at the cathode-facing edge. It is also possible that they are involved in externalization of newly synthesized AChR at the cathode-facing cell surface, as the participation of these in field-induced AChR aggregation has not been excluded. However, each of these elements was observed only at a minority of the dense areas, and their potential involvement in any AChR aggregation event remains a matter for further study.

The exposure to a DC electric field could be expected to influence the cell in a number of ways, including electrophoresis of surface components, extracellular electro-osmotic flow, membrane depolarization, gradient formation, etc. This study does not indicate which of these influences are important in AChR aggregation, and the means by which the field effects this process is, as is the case for nerve-induced receptor aggregation, a matter of speculation. However, a number of similarities between nerve and field-induced AChR aggregation are apparent: (*a*) Both cause the redistribution of preexisting AChR into localized areas of the sarcolemma (3); (*b*) both result in the formation of distinct AChR clusters with a substructure in the micrometer-to-submicrometer range (56); (*c*) both result in the stabilization of AChR against lateral diffusion (13, 15); (*d*) both result in the formation of structural specializations in association with the receptor aggregate; and (*e*) both occur in a similar time span (25). Thus, it seems likely that the two influences are activating the same aggregation mechanism. We anticipate that further studies using the electric field system, which is easily controlled in terms of the site and timing of AChR aggregation, will clarify the events involved in this phenomenon.

We thank Kevin A. Phelan for expert technical assistance.

This research was supported by National Institutes of Health grant NS16259 and a grant from the Muscular Dystrophy Association.

Send reprint requests to Dr. Peng.

Received for publication 22 March 1984, and in revised form 23 August 1984.

REFERENCES

1. Bevan, S., and J. H. Steinbach. 1977. The distribution of α-bungarotoxin binding sites on mammalian skeletal muscle *in vivo*. *J. Physiol.* (Lond.).267:195–213.
2. Braithwaite, A. W., and A. J. Harris. 1979. Neural influence on acetylcholine receptor clusters in embryonic development of skeletal muscles. *Nature* (*Lond.*). 279:549–551.
3. Anderson, M. J., and M. W. Cohen. 1977. Nerve-induced and spontaneous redistribution of acetylcholine receptors on cultured muscle cells. *J. Physiol.* (Lond.). 268:757–773.
4. Kullberg, R. W., T. L. Lentz, and M. W. Cohen. 1977. Development of the myotomal neuromuscular junction in *Xenopus laevis*: an electophysiological and fine-structural study. *Dev. Biol.* 60:101–129.
5. Jacob, M., and T. L. Lentz. 1979. Localization of acetylcholine receptors by means of horseradish peroxidase-α-bungarotoxin during formation and development of the neuromuscular junction in the chick embryo. *J. Cell Biol.* 82:195–211.
6. Peng, H. B., Y. Nakajima, and P. C. Bridgman. 1980. Development of the postsynaptic membrane in *Xenopus* neuromuscular cultures observed by freeze-fracture and thin-section electron microscopy. *Brain Res.* 196:11–31.
7. Fertuck, H. C., and M. M. Salpeter. 1974. Localization of acetylcholine receptor by ^{125}I-labeled α-bungarotoxin binding at mouse motor end plates. *Proc. Natl. Acad. Sci. USA.* 71:1376–1378.
8. Lentz, T. L., J. E. Mazurkiewicz, and J. Rosenthal. 1977. Cytochemical localization of acetylcholine receptors at the neuromuscular junction by means of horseradish peroxidase-labeled α-bungarotoxin. *Brain Res.* 132:423–442.
9. Burrage, T. G., and T. L. Lentz. 1981. Ultrastructural characterization of surface specializations containing high-density acetylcholine receptors on embryonic chick myotubes *in vivo* and *in vitro*. *Dev. Biol.* 85:267–286.
10. Salpeter, M. M., S. Spanton, K. Holley, and T. R. Podleski. 1982. Brain extract causes acetylcholine receptor redistribution which mimics some early events at developing neuromuscular junctions. *J. Cell Biol.* 93:417–425.
11. Peng, H. B., and P.-C. Cheng. 1982. Formation of postsynaptic specialization induced by latex beads in cultured muscle cells. *J. Neurosci.* 2:1760–1774.
12. Stya, M., and D. Axelrod. 1983. Diffusely distributed acetylcholine receptors can participate in cluster formation on cultured rat myotubes. *Proc. Natl. Acad. Sci. USA.* 80:449–453.
13. Axelrod, D., P. Ravdin, D. E. Kopple, J. Schlessinger, W. W. Webb, E. L. Elson, and T. R. Podleski. 1976. Lateral motion of fluorescently labeled acetylcholine receptors in membranes of developing muscle fibers. *Proc. Natl. Acad. Sci. USA.* 73:4594–4598.
14. Poo, M.-M. 1982. Rapid lateral diffusion of functional ACh receptors in embryonic muscle membrane. *Nature* (*Lond.*). 295:332–334.

15. Orida, N., and M.-M. Poo. 1978. Electrophoretic movement and localization of acetylcholine receptors in the embryonic muscle cell membrane. *Nature (Lond.)*. 275:31–35.
16. McLaughlin, S., and M.-M. Poo. 1981. The role of electroosmosis in the electric field-induced movement of charged macromolecules on the surfaces of cells. *Biophys. J.* 34:85–93.
17. Luther, P. W., and H. B. Peng. 1983. Membrane specializations associated with electric field-induced AChR clusters. *J. Cell Biol.* 97(5, Pt. 2):238*a*. (Abstr.)
18. Nieuwkoop, P. D., and J. Faber. 1967. Normal Table of *Xenopus laevis* (Daudin). Elsevier/North-Holland Biomedical Press, Amsterdam. Second ed. 252 pp.
19. Anderson, M. J., M. W. Cohen, and E. Zorychta. 1977. Effects of innervation on the distribution of acetylcholine receptors on cultured muscle cells. *J. Physiol. (Lond.)*. 268:731–756.
20. Peng, H. B., and Y. Nakajima. 1978. Membrane particle aggregates in innervated and noninnervated cultures of *Xenopus* embryonic muscle cells. *Proc. Natl. Acad. Sci. USA*. 75:500–504.
21. Ravdin, P., and D. Axelrod. 1977. Fluorescent tetramethyl rhodamine derivatives of α-bungarotoxin. Preparation, separation and characterization. *Anal. Biochem.* 80:585–592.
22. Olek, A. J., P. A. Pudimat, and M. P. Daniels. 1983. Direct observation of the rapid aggregation of acetylcholine receptors on identified cultured myotubes after exposure to embryonic brain extract. *Cell*. 34:255–264.
23. Peng, H. B., and L. F. Jaffe. 1976. Polarization of fucoid eggs by steady electric fields. *Dev. Biol.* 53:277–284.
24. Poo, M.-M., J. W. Lam, N. Orida, and A. W. Chao. 1979. Electrophoresis and diffusion in the plane of the cell membrane. *Biophys. J.* 26:1–22.
25. Cohen, M. W. 1980. Development of an amphibian neuromuscular junction *in vivo* and in culture. *J. Exp. Biol.* 89:43–56.
26. Hirokawa, N., and J. E. Heuser. 1982. Internal and external differentiations of the postsynaptic membrane of the neuromuscular junction. *J. Neurocytol.* 11:487–510.
27. Ellisman, M. H., J. E. Rash, L. A. Staehelin, and K. R. Porter. 1976. Studies of excitable membranes. II. A comparison of specializations at neuromuscular junctions and non-junctional sarcolemmas of mammalian fast and slow twitch muscle fibers. *J. Cell Biol.* 68:752–774.
28. Peng, H. B. 1983. Cytoskeletal organization of the presynaptic nerve terminal and the acetylcholine receptor cluster in cell cultures. *J. Cell Biol.* 97:489–498.
29. Rosenbluth, J. 1974. Substructure of amphibian motor endplate. Evidence for a granular component projecting from the outer surface of the receptive membrane. *J. Cell Biol.* 62:755–766.
30. Rash, J. E., C. S. Hudson, and M. H. Ellisman. 1978. Ultrastructure of acetylcholine receptors at the mammalian neuromuscular junction. *In* Cell Membrane Receptor for Drugs and Hormones: A Multidisciplinary Approach. R. W. Strauband and L. Bolis, editors. Raven Press, New York. 47–68.
31. Heuser, J. E., and S. R. Salpeter. 1979. Organization of acetylcholine receptors in quick-frozen, deep-etched and rotary-replicated *Torpedo* postsynaptic membrane. *J. Cell Biol.* 82:150–173.
32. Hall, Z. W., B. W. Lubit, and J. H. Schwartz. 1981. Cytoplasmic actin in postsynaptic structures at the neuromuscular junction. *J. Cell Biol.* 90:789–792.
33. Bloch, R. J., and Z. W. Hall. 1983. Cytoskeletal components of the vertebrate neuromuscular junction: vinculin, α-actinin, and filamin. *J. Cell Biol.* 97:217–223.
34. Burden, S. 1982. Identification of an intracellular postsynaptic antigen at the frog neuromuscular junction. *J. Cell Biol.* 94:521–530.
35. Rash, J. E., and M. H. Ellisman. 1974. Studies of excitable membranes. I. Macromolecular specializations of the neuromuscular junction and the nonjunctional sarcolemma. *J. Cell Biol.* 63:567–586.
36. Tank, D. W., E.-S. Wu, and W. W. Webb. 1982. Enhanced molecular diffusibility in muscle membrane blebs: release of lateral constraints. *J. Cell Biol.* 92:207–212.
37. Prives, J., A. B. Fulton, S. Penman, M. P. Daniels, and C. N. Christian. 1982. Interaction of the cytoskeletal framework with acetylcholine receptor on the surface of embryonic muscle cells in culture. *J. Cell Biol.* 92:231–236.
38. Connolly, J. A. 1983. ACh receptor/cytoskeleton interactions in primary muscle cells. *J. Cell Biol.* 97(5, Pt. 2):238*a*. (Abstr.)
39. Bloch, R. J. 1983. Acetylcholine receptor clustering in rat myotubes: requirement for calcium and effects of drugs which depolymerize microtubules. *J. Neurosci.* 3:2670–2680.
40. Sanes, J. R., and Z. W. Hall. 1979. Antibodies that bind specifically to synaptic sites on muscle fiber basal lamina. *J. Cell Biol.* 83:357–370.
41. Silberstein, L., N. C. Inestrosa, and Z. W. Hall. 1982. Aneural muscle cell cultures make synaptic basal lamina components. *Nature (Lond.)*. 295:143–145.
42. Anderson, M. J., and D. M. Fambrough. 1983. Aggregates of acetylcholine receptors are associated with plaques of a basal lamina heparan sulfate proteoglycan on the surface of skeletal muscle fibers. *J. Cell Biol.* 97:1396–1411.
43. Burden, S. J., P. B. Sargent, and U. J. McMahan. 1979. Acetylcholine receptors in regenerating muscle accumulate at original synaptic sites in the absence of nerve. *J. Cell Biol.* 82:412–425.
44. Wallace, B. G., E. W. Godfrey, R. M. Nitkin, L. L. Rubin, and U. J. McMahan. 1982. An extract of extracellular matrix fraction that organizes acetylcholine receptors. *In* Muscle Development: Molecular and Cellular Control. M. L. Pearson and M. F. Epstein, editors. Cold Spring Harbor Laboratories, Cold Spring Harbor, New York. 469–479.
45. Singer, I. I. 1979. The fibronexus: a transmembrane association of fibronectin-containing fibers and bundles of 5 nm microfilaments in hamster and human fibroblasts. *Cell*. 16:675–685.
46. Shear, C. R., and R. J. Bloch. 1983. Subsarcolemmal densities in chicken skeletal muscle are rich in vinculin. *J. Cell Biol.* 97(5, Pt. 2):258*a*. (Abstr.)
47. Nakao, T. 1976. Some observations on the fine structure of the myotendinous junction in myotomal muscles of the tadpole tail. *Cell. Tissue Res.* 166:241–254.
48. Betz, W. 1976. Functional and non-functional contacts between ciliary neurons and muscle grown *in vitro*. *J. Physiol. (Lond.)*. 254:75–86.
49. Jones, R., and G. Vrbova. 1974. Two factors responsible for the development of denervation hypersensitivity. *J. Physiol. (Lond.)*. 236:517–538.
50. Vogel, Z., C. N. Christian, M. Vigny, H. C. Bauer, P. Sonderegger, and M. P. Daniels. 1983. Laminin induces acetylcholine receptor aggregation on cultured myotubes and enhances the receptor aggregation activity of a neuronal factor. *J. Neurosci.* 3:1058–1068.
51. Edwards, C., and M. L. Frisch. 1976. A model for the localization of acetylcholine receptors at the muscle endplate. *J. Neurobiol.* 7:377–381.
52. Bloch, R. J. 1979. Dispersal and reformation of acetylcholine receptor clusters of cultured rat myotubes treated with inhibitors of energy metabolism. *J. Cell Biol.* 82:629–643.
53. Rees, R. P. 1978. Inclusion in coated vesicle membrane as the transport mechanism for acetylcholine receptor molecules in isolated cultured sympathetic neurons. *J. Cell Biol.* 79(2, Pt. 2):99*a*. (Abstr.)
54. Bursztajn, S., and G. D. Fischbach. 1984. Evidence that coated vesicles transport acetylcholine receptors to the surface membrane of chick myotubes. *J. Cell Biol.* 98:498–506.
55. Weldon, P. R., F. Moody-Corbett, and M. W. Cohen. 1981. Ultrastructure of sites of cholinesterase activity on amphibian embryonic muscle cells cultured without nerve. *Dev. Biol.* 84:341–350.
56. Steinbach, J. H. 1981. Development changes in acetylcholine receptor aggregates at rat neuromuscular junctions. *Dev. Biol.* 84:267–276.